Hexacyanometallate aqueous flow battery

Ji-Eun Jang
Ulsan National Institute of Science and Technology
Ryeong-ah Kim
Ulsan National Institute of Science and Technology
Chanhee Lee
Ulsan National Institute of Science and Technology
Sujin Kang
Ulsan National Institute of Science and Technology
Jaechan Ryu
Ulsan National Institute of Science and Technology
S. Jayasubramaniyan
Ulsan National Institute of Science and Technology
Jaephil Cho
Ulsan National Institute of Science and Technology https://orcid.org/0000-0002-3890-1432
Wonyoung Choe
Ulsan National Institute of Science and Technology https://orcid.org/0000-0003-0957-1187
Dong-Hwa Seo
Ulsan National Institute of Science and Technology https://orcid.org/0000-0002-7200-7186
Hyun-Wook Lee (hyunwooklee@unist.ac.kr)
Ulsan National Institute of Science and Technology https://orcid.org/0000-0001-9074-1619

Article

Keywords: redox flow batteries (RFBs), energy storage

Posted Date: June 15th, 2021

DOI: https://doi.org/10.21203/rs.3.rs-568177/v1

Abstract

Aqueous redox flow batteries (RFBs) have attracted significant attention as energy storage systems by virtue of their inexpensive nature and long-lasting features. Although all-vanadium RFBs exhibit long lifetimes, the cost of vanadium resources fluctuates considerably, and is generally expensive. Iron–chromium RFBs take advantage of utilizing a low-cost and large abundance of iron and chromite ore; however, the redox chemistry of $Cr^{II/III}$ generally involves strong Jahn–Teller effects. Herein, we introduce a new Cr-based negolyte coordinated with strong-field ligands capable of mitigating strong Jahn–Teller effects, thereby facilitating low redox potential, high stability, and rapid kinetics. Density functional theory (DFT) calculations reveal that the complex of $[Cr(CN)_6]^{4-}$ prefers low-spin states, facilitating a stable and fast redox reaction. The prototype full-cell configuration features a high-energy density of 11.4 Wh L^{-1} and a stable lifetime of 250 cycles. Consequently, our proposed system opens new avenues for the development of high-performance RFBs.

Introduction

Sustainable energy storage systems (ESSs) have received a great deal of attention to satisfy emerging demands at grid-scale without compensation for large-scale and long-time operation; additionally, they have low maintenance and cost [1,2]. However, the current lithium-ion battery (LIB) technology might not be chosen as an ideal candidate to replace active materials in the positive and negative electrodes in grid energy storage because faded LIBs result from the degradation of active materials (cathode and anode) or the dried electrolyte. Maintenance of LIBs incur relatively high costs and involve complicated processes. In this regard, aqueous redox flow batteries (RFBs) have been widely employed as an alternative for economical ESSs [3]. One noticeable advantage of aqueous systems is their very high dielectric constant, allowing soluble redox couples to dissolve with large quantities in an aqueous solution with dissociation. The high solubility also benefits to increase the available energy densities and the output current would be controlled by the size of the electrode stacks in RFBs. Of course, aqueous systems are advantageous in many aspects of: they are inexpensive, environmentally benign, and highly soluble rather than the use of organic liquid systems [4]. As shown in Fig. 1a replacing or rebalancing negolytes and posolytes can be readily altered while maintaining infra-tank and pump systems; such properties are well-suited for stationary energy storage [5]. All-vanadium redox flow batteries (VRFB) have been widely studied since the same elements are employed in both the negolyte ($V^{II/III}$) and posolyte ($V^{IV/V}$) and since such systems feature long calendar and cycle lives with more than 200,000 cycles [6,7]. Nevertheless, the price of vanadium source, V_2O_5, has been highly fluctuated up to 28.8 USD/lb at the end of 2018, resulting in high costs and performance as 1,000 USD/kWh approximately [8].

The concept of iron-chromium RFBs using ferrous/ferric ($Fe^{II/III}$) and chromous/chromic ($Cr^{II/III}$) ions is the first chemistry taking advantage of low cost and widely abundant iron and chromite ore [2,9,10]. These $Fe^{II/III}$ redox couples are expected to be more stable as a posolyte with a combination of cyanide ligands

that have extensively used to a posolyte material in RFB reference [11–14]. However, the redox chemistry of $Cr^{II/III}$ in chromium-based negolytes generally involves strong Jahn-Teller effects due to the unequal occupation of electrons in e_g orbitals of high-spin Cr^{II} (d^4) as shown in Fig. 1b. This can lead to simultaneous splitting of the electronic states and a symmetry-lowering distortion. This phenomenon limits the electrochemical reactions as a low current density and energy efficiency, resulting in the sluggish kinetics of the $Cr^{II/III}$ redox couple ($k_0 < 10^{-6}$) [14–17] and low Coulombic efficiency, which is corroborated by a severe hydrogen evolution reaction (HER) arising from the low reduction potential (-0.41 V vs. SHE) under acidic conditions [18]. Interestingly, the d^4 electron configuration of Cr^{II} can alter its spin states from high-spin to low-spin depending on the increase of the energy gap (Δ_o) between e_g and t_{2g} orbitals. Coordination compounds composed of a metal ion and ligands offer the benefit of pi (π) interactions, which facilitate dramatic effects on the triply degenerate t_{2g} orbitals. Ligands such as carbonyls (CO) and cyanides (CN^-) are π acceptors with empty orbitals that can interact with metal d orbitals in a π fashion, leading to the stabilization of t_{2g} orbitals. It has been suggested that the significant electronic stabilization is beneficial to stable $Cr^{II/III}$ redox reactions enabled by the low-spin configuration of Cr^{II}. As shown in Fig. 1c, the energy split between e_g and t_{2g} orbitals can increase from the free metal ion state to coordination with a strong-field ligand, playing a crucial role in shifting a redox potential more negative figures according to spectrochemical series [19]. In particular, when Cr^{III} changes its oxidation state to Cr^{II} at a high-spin state, electrons are transferred into the e_g orbitals, whereas electron transfer can occur into t_{2g} orbitals in the coordination complex covalent with strong-field ligand**s,** manipulating the redox potential of $Cr^{II/III}$ *via* the use of suitable ligands and simultaneously mitigating strong Jahn-Teller effects.

Although various studies have provided some negolytes in a chromium-based system, there is a need for negolytes containing low-redox-potential with fast kinetics and stable cyclability [13,14,20–22]. Bae *et al.* showed that chromium-ethylenediaminetetraacetic acid (Cr-EDTA) can exhibit a low reduction potential (-0.99 V vs. SHE) with reversible cathodic and anodic processes. However, the designed battery have shown slow kinetics operated at very low current density of 2.5 mA cm^{-2}, and a very low energy efficiency of less than 7% [20,21] due to the large overpotential of chromium-based redox couples. Slow kinetics inhibit the power density of batteries and occur in the comparable reaction of hydrogen evolution, although chromium complexes have merits of low redox potential, allowing for an overall high voltage. Marshak *et al.* introduced 1,3-propylenediaminetetraacetic acid chelated chromium (Cr-PDTA) as a negolyte material using a strategy of chelating ligands. The full-cell couple with the posolyte, $[Fe(CN)_6]^{4-/3-}$ showed a high discharging potential of approximately 1.5 V and an improved the energy efficiency of 78.1% during cycling at ±100 mA cm^{-2}, which provides the best performance among the new chromium-based RFBs. However, such cycle life of 70 still needs to be ameliorated. Chen *et al.* found various chromium complexes for Cr-based RFBs, such as Cr-bipyridine ($[Cr(bipy)_2(H_2O)_2]^{3-}$), Cr-dipicolicic acid ($[Cr(DPA)_2]^-$), Cr-iminodiacetate ($[Cr(IDA)_2]^-$), and chromium 3-((2,6- bis (ethoxycarbonyl) pyridin-4-yl)oxy)-N,N,N-trimethylpropan-1-aminium bromide ($[Cr(f\text{-}DPA)_2]^+$) [14]. This work assessed that the

charge transfer kinetics, stability, and solubility of a complex would be corroborated by the suitable molecular design. Therefore, the better designs of material chemistry are indubitably required in order to resolve the performance issues associated with the aforementioned systems.

In this work, we introduce a new Fe-Cr RFB system coordinated by strong-field cyanide ligands to mitigate strong Jahn-Teller effects for high-energy and stable performances. Chromium complexes coordinated with strong-field cyanides can allow low redox potentials compared to complexes coordinated with weak-field ligands due to the electron transfer to t_{2g} orbitals rather than e_g orbitals. Since this system is introduced for the first time, we have carefully evaluated diverse assessment methods for the unique features with low redox potential, high stability, and fast kinetics below the potential of hydrogen evolution reactions as shown in Fig. 2a. A thermodynamic analysis of the redox reaction energetics using density functional theory (DFT) calculations suggests that the $[Cr(CN)_6]^{4-}$ complex is preferentially associated with low-spin states relative to complexes coordinated with weak-field ligands, facilitating a stable and fast redox reaction. In order to enable further development of redox flow system, we matched the negolyte with a $K_3[Fe(CN)_6]$ posolyte as a full cell and performed various investigations to confirm the proper redox at different SOCs. Benefiting from the aforementioned uniqueness, this hexacyanometalate-based RFB is capable of reversible redox reactions with relatively high potential as an aqueous system taking advantage of the low potential of $[Cr(CN)_6]^{4-/3-}$ and improved cycling performance at high current densities. Furthermore, we expand on the considerable degradation mechanisms that play a crucial role in governing the kinetics and stability of the reaction and provide important insights into the design of a stable RFB.

Results

Electrochemical properties of hexacyanochromate with respect to low redox potential, high stability, and fast kinetics

Facile synthetic $K_3[Cr(CN)_6]$ was employed as a source of $[Cr(CN)_6]^{4-/3-}$ in our experiment; this enabled us to take advantage of the low chemical cost of chromium(III) acetate, which is beneficial compared to the onerous price of commercially available $K_3[Cr(CN)_6]$ (Sigma Aldrich, 99.99%). X-ray diffraction (XRD) profiles in Supplementary Fig. 1 reveal that as-synthesized $K_3[Cr(CN)_6]$ corresponds to the XRD patterns of both commercialized $K_3[Cr(CN)_6]$ and PDF 00-027-1350. Cyclic voltammograms (CVs) in Fig. 2a,b show reversible redox reactions of $[Cr(CN)_6]^{4-/3-}$ anions, which possess the reduction and oxidation peaks at -1.19 and -1.11 V vs. SHE, respectively. Whereas CV of $Cr^{II/III}$ in $CrCl_3$ redox reaction denotes serious irreversibility with a considerably small oxidation peak near -0.11 V and a negligible reduction peak, even at the same scan rate of 20 mV s^{-1}. The $CrCl_3$ reaction also shows poor activity with very low current density. The reliable electrochemical properties of $[Cr(CN)_6]^{4-/3-}$ are unique because of its low redox potential of approximately -1.15 V, which is lower than the potential of HERs in an aqueous system. The redox potential could arise from complexation effects, leading to the stabilization of the energy level of

t_{2g} orbitals in the complex [19]. Simultaneously, controlling supporting electrolytes facilitate redox reactions with high stability and fast kinetics. To validate the plausible properties of $[Cr(CN)_6]^{4-/3-}$, various aspects influencing such formidable properties are needed to discuss in more detail in the next section.

Hexacyanometallates are known to be more stable at acidic pH than basic pH due to the ligand exchange of CN^- to OH^-, resulting in the destruction of the hexacyanometallates [23]. This ligand exchange is the dominant loss mechanism during electrochemical reactions in RFBs, thereby the condition mitigating this ligand exchange is suggested to extend their lifetimes. However, reductive electrolysis to hydrogen could occur at higher potential in acid, which in turn limits the use of negolytes with low reaction potentials. Supporting electrolytes can open up new opportunities to suppress undesirable ligand exchanges during the reaction. For example, high concentrations of supporting electrolytes limit trace solubility, potentially extending the cathodic electrochemical stability window of water beyond the thermodynamic level of -0.8 V vs. SHE [24]. In addition, concentrated supporting electrolytes decrease the chemical activity of water, resulting in less ligand exchange to OH^-. As a cyanide-based supporting electrolyte, sodium cyanide was selected for the excellent electrochemical stability, especially against very reductive potentials, combined with a high solubility in water. Long-term CV data in Fig. 2c,d compares the stability of $[Cr(CN)_6]^{4-/3-}$ redox reactions in the cyanide-based supporting electrolyte (NaCN) to the NaCl supporting electrolyte. The initial cycles using both NaCl and NaCN supporting electrolytes in Fig. 2c,d clearly show the reversible reduction and oxidation reactions near -1.2 and -1.1 V, respectively. Whereas the current density when using the NaCl electrolyte rapidly diminished and was rarely detected after 70 cycles, suggesting that the NaCl supporting electrolyte did not alleviate the ligand exchange and the redox species might result in forming $Cr(OH)_x$ *via* side reactions; such material might be deposited on the glassy carbon electrode [25]. On the other hand, the current density and redox potentials using NaCN supporting electrolyte were maintained even after 500 cycles as shown in Fig. 2d, which was expected since the ligand exchange was limited by the number of cyanide ligands. Unlike the chloride based solutions, the excessive cyanide ions played a significant role in suppressing decomposition and maintaining a high stability of $[Cr(CN)_6]^{4-/3-}$.

The fast kinetics of electrochemical reactions can be understood by analyzing associations between the CV scan rate and the corresponding current density as shown in Fig. 2e,f. The CV data, which were scanned from 5-500 mV s^{-1}, show small potential shifts from 81-134 mV (Fig. 2e and Supplementary Table 1) and exhibit high current densities during redox processes, even at the high scan rate of 500 mV s^{-1}, indicative of a stable redox system with high charge and discharge conditions. The corresponding peak currents exhibit a linear relationship with respect to the square root of the scan rates as shown in Fig. 2f; this means that the $[Cr(CN)_6]^{4-/3-}$ redox couple has a quasi-reversible electrochemical property. The small ΔE_p is comparable with the value in the diffusion-controlled kinetic regime such that the slope in Fig. 2f can thus be used to determine the diffusion coefficient (D_0) *via* the Randles-Sevcik equation. Since the slopes of the cathodic and anodic processes are ±0.0002, the diffusion coefficient D_0 is calculated as 7.16×10^{-6} cm^2 s^{-1}. The charge transfer rate (k^0) can also be calculated using the Nicholson method that provides the information about the relationship between ΔE_p and k^0 (Table S2) [26]. According to this

method, the k_0 is calculated as 6.03 × 10^{-3} cm s^{-1}, facilitating that $[Cr(CN)_6]^{4-/3-}$ redox couples show outstanding performance without any catalysts compared to other Cr-based materials [18,20–22]. Table S3 compares the electrochemical properties of the reduction potential, diffusion coefficient, and charge transfer rate in the hexacyanochromate complex with those obtained by previous studies. In particular, k^0 of $[Cr(CN)_6]^{4-/3-}$ redox couple is approximately 6,000 times higher than $Cr^{II/III}$ redox couple in $CrCl_3$ without catalysts and even six times higher than that with Bi catalyst. Additionally, it is higher than that of $Cr^{II/III}$-PDTA redox couple (1.7×10^{-4} cm s^{-1}), which had previously been considered to have the best performance among Cr-based systems. Our electrochemical analyses of the $[Cr(CN)_6]^{4-/3-}$ complex indicate that it exhibits desirable behavior that enables fast kinetics with high stability at low redox potentials below the hydrogen evolution reaction, which can be a promising candidate as a negolyte for sustainable RFB systems.

Simulated electronic configurations, Jahn-Teller distortions, and redox reaction energies of Cr^{II}-based compounds. a, Energy levels of electronic orbitals. Upward arrows represent electrons with up-spin and downward arrows represent electrons with down-spin. Black solid and dashed lines denote occupied molecular orbitals (MOs) for up-spin and down-spin, respectively. Blue solid and dashed lines indicate unoccupied MOs for up-spin and down-spin, respectively. **b,** Molecular structures with bond lengths of ligands and distortion index *D* of octahedral complex. **c,** Calculated energy changes during $Cr^{II/III}$redox reactions in these compounds.

Theoretical consideration by DFT simulation of chromium-based compounds

We performed molecular simulations to understand the complex chemistry behind the stable redox reaction of the $[Cr(CN)_6]^{4-/3-}$ coordination compound at low potential. By calculating the electronic structures and redox reaction energies of various Cr^{II}-ligand complexes using density functional theory (DFT), we revealed the complex interplay between ligands and electronic structure in governing redox potential. Since frontier molecular orbitals (MOs), including the highest occupied and lowest unoccupied MOs, are important for the redox behaviors of coordination compounds, we compared electronic configurations of the frontier MOs of representative Cr^{II}-based compounds using DFT calculation as presented in Fig. 3a. We considered triplet (t_{2g}^4) and quintet ($t_{2g}^3 e_g^1$) states for each Cr^{II}-based compound in order to find the energetic stable spin states (Table S4). $[CrCl_6]^{4-}$, $[Cr(H_2O)_6]^{2+}$, and $[Cr(NH_3)_6]^{2+}$ are stable in their quintet states (high-spin state), whereas $[Cr(CN)_6]^{4-}$ is stable in its triplet states (low-spin state); these finding are consistent with conventional understanding that strong-field ligands such as CN^- result in low-spin states due to their large *d* orbital splitting.

Since the Cr^{II}-based compounds with high-spin state have single electron at e_g states, thereby leading to strong Jahn-Teller distortions, bonds with two ligands along *z* direction are more elongated than the bonds with other fours, as shown in Fig. 3b. In contrast, $[Cr(CN)_6]^{4-}$ has weak Jahn-Teller distortions due to unevenly occupied t_{2g} orbitals in the low-spin state, allowing for negligible elongation of bonds along

the *z* direction. To compare distortion degree, we calculated the distortion index using the following equation:

$$d = \frac{1}{n}\sum_{i=1}^{n}\frac{|l_i - l_{av}|}{l_{av}}$$

where l_i is the distance from the central Cr atom to the i^{th} ligand and l_{av} is the average distance. $[CrCl_6]^{4-}$ has a larger distortion index of 0.2599 than others with a high-spin state because of its negatively charged ligands, which is in agreement with strong stabilization of the highest occupied e_g state in Fig. 3a. $[Cr(CN)_6]^{4-}$ has the smallest distortion index of 0.007 due to weak Jahn-Teller effects. It is thus inferred that the fast kinetics of the $[Cr(CN)_6]^{4-}$ negolyte is mainly attributed to its facile redox reaction with weak Jahn-Teller distortion. We further calculated energy changes in these compounds during $Cr^{II/III}$ redox reactions. As shown in Fig. 3c, $[Cr(CN)_6]^{4-/3-}$ has a much lower energy change than other compounds, explaining its low potential in our experimental results (Fig. 2a). Our DFT calculations show that the coordination compound of $[Cr(CN)_6]^{4-/3-}$ possesses stable and fast redox reactions at a low potential of -1.15 V, which is enabled by the low-spin configuration of Cr^{II}.

Full redox flow battery using hexacyanometallates

After carefully validating the desirable properties, we built a full RFB cell composed of $[Cr(CN)_6]^{4-/3-}$ and $[Fe(CN)_6]^{4-/3-}$ redox couples as shown in Fig. 1a and Supplementary Fig.2. The preliminary half-cell data in Fig. 2a uggest that the standard thermodynamic potential of the two negolyte and posolyte is 1.64 V. However, it is notorious that a half-cell CV test does not always correlate to full-cell data measured in a constant current mode because the potential-derived characterization is imprecise due to the overlapped faradaic response for the forward process, especially in the potential regime below HER. In this regard, we have verified the galvanostatic profile for the full-cell configuration, showing a highly reversible capacity of 10,200 mAh L^{-1} at a discharging current density of 50 mA cm^{-2} with an average potential of 1.43V (Fig. 4a. In particular, the redox mediators of $[Cr(CN)_6]^{4-/3-}$ are coordination compounds that are well known to exhibit vivid colors depending on the *d* orbital energy gap of transition metals. During the discharge process, the color of the negolyte in Fig. 4a changes from dark brown to light red, as also shown in Supplementary Movie S1. The UV-vis spectra depending on the state of charge (SOC), shown in Fig. 4b, also reveals corresponding species such that the peak at 326 nm indicates the charged state of $[Cr(CN)_6]^{4-}$ [27–29]. As the color changes to light red, the correlated peaks at 307 and 377 nm increase together with increased concentrations of $[Cr(CN)_6]^{3-}$, implying that comprehensive redox change

occurred in the full-cell configuration with excellent reductive stability. Another post-mortem XRD analysis also manifests successful conversion to $[Cr(CN)_6]^{4-}$ as shown in Fig. 4c. We used dried powder obtained by evaporating solvent of the negolyte at the different SOCs of 0, 50, and 100 %. Asterisks (*) in Fig. 4c indicate the information of sodium cyanide (NaCN) reference, which was exploited to calibrate peak positions across different samples. The enlarged XRD patterns at 32-35 degrees in Fig. 4c clearly elucidate that the dried samples show good agreement with the conventional $K_3[Cr(CN)_6]$ and $K_4[Cr(CN)_6]$ phases upon the SOCs, implying a successful phase transition from $[Cr(CN)_6]^{4-}$ to $[Cr(CN)_6]^{3-}$.

Cell polarization curves and power densities in Fig. 4d, E enable to the fast kinetics of $[Cr(CN)_6]^{4-/3-}$ to be deduced for the full-cell configuration. This advance allows accurate demonstration of the electrochemical behavior of $[Cr(CN)_6]^{4-/3-}$ as well as the implementation of hexacyanometallates for a genuine energy storage application with competitive performance. Using our characterization of the current-voltage behavior at various SOC values (0 %, 10 %, 25 %, 75 %, and 100 %), we achieved a remarkable performance of $[Cr(CN)_6]^{4-/3-}$ even without using any catalysts, such as bismuth, titanium, or a porous current collector, especially at high current densities above 700 mA cm^{-2} [30–33]. Furthermore, the maximum peak power density reaches 410 mW cm^{-2} as shown in Fig. 4e, denoting that the material is a promising candidate for large-scale energy storage field. This charge transfer kinetics in the full-cell configuration does not seem to limit power output, which is in good agreement with the rapid kinetics presented in Fig. 2e,f. Finally, we tested the long-term cycling performance of the full-cell composed of $[Cr(CN)_6]^{4-/3-}$ and $[Fe(CN)_6]^{4-/3-}$ complexes at a current density of 100 mA cm^{-2} (Fig. 4f and Supplementary Fig. 3). No obvious decay occurred with respect to Coulombic efficiency, energy efficiency, and normalized capacity for 250 cycles. Coulombic efficiency is another vital factor for evaluating the electrochemical performance of hexacyanometallates because it determines the reversibility of the redox processes and the inactivity of HER. The Coulombic efficiencies of the hexacyanometallates present above 99% to 250 cycles, inferring the truly reversible reaction of redox mediators. The energy efficiency was also maintained to 76-77% attributed by overpotential between charge and discharge at the high current density. The capacity decay was calculated to be less than 0.02% per cycle, denoting that there are no significant side reactions such as fatal decomposition of active materials or HER. Based on these tests, we have confirmed that the fast kinetics with high stability continuously occur from $[Cr(CN)_6]^{4-/3-}$ and $[Fe(CN)_6]^{4-/3-}$ complexes, enabling the stable operation of even the full-cell system. Our results show that the full cell exhibits a prolonged cycle life with promising electrochemical properties, which are compared to previous results in Table S5.

Discussion

For a complete assessment of the study materials for practical applications, we have to consider the significant degradation mechanisms of RFBs, such as crossover, self-decomposition of active materials, and electrolyte side reaction [5]. Crossovers denote the ion-transport of active electrolytes across ion-conducting membranes leading to undesirable migration of ions in posolytes, negolytes, and/or

supporting electrolytes. In this work, we employed a cation-exchanged Nafion membrane that transports mobile cations and excludes the negatively charged anions either by size or Donnan exclusion effects (Fig. 1a). Since $[Cr(CN)_6]^{4-/3-}$ and $[Fe(CN)_6]^{4-/3-}$ hexacyanometallates are surrounded by strong-field ligands of cyanides, the outer region of the octahedral redox species is strongly negative, resulting in complete exclusion dominated by electrostatic interactions within the membrane. Bakajin *et al.* measured ion exclusion coefficients using the Donnan model, suggesting that $K_3Fe(CN)_6$ showed near-complete exclusion due to its high cation-anion valence (1/3), which indicates high electrostatic repulsion [34]. The self-decomposition of active materials and electrolyte side reactions should also be considered for stable RFBs since the chemical decomposition of redox species causes deterioration of the intrinsic property of active materials. $[Fe(CN)_6]^{4-/3-}$ is widely used as a reference posolyte due to its highly stable performance without compromising the self-decomposition of active materials. In the case of $[Cr(CN)_6]^{4-/3-}$, we observed that the charged state of $[Cr(CN)_6]^{4-}$ tends to partially exchange cyanide with hydroxyl (OH^-) ligands *via* photoaquation mechanism, which is well-known in metal complexes [27–29] (Supplementary Fig. 4a). It is also known that the photo-excitation of the hexacyanometallates might lead either to its dissociation into CN^- and $[Cr(CN)_5]^{3-}$ fragments or the formation of $[Cr(CN)_5(H_2O)]^{3-}$ in a general aqueous medium[29,35]. However, cyanide complexes tend to show different features depending on the solvent interaction, thereby influencing the electronic structure. A feasible mechanism of ligand stability in this system is that the cyanide-based supporting electrolyte can offer an opportunity to control the condition of the aqueous solvent. As shown in Supplementary Fig. 4b, although as-synthesized $K_3Cr(CN)_6$ is coordinated with aqua ligands observed in UV-vis spectra, the subsequent complex after first cycle verifies ligand exchange to cyanides forming $K_3Cr(CN)_6$ [28,29]. Our results provide clear examples both of the energy dependence of ligand exchanges and of the role of supporting electrolytes in the reactivity of metal complexes. We therefore conclude that by harnessing this advantage, the suggested RFB system can operate the prolonged cycles without crossover problems and chemical decomposition, including ligand exchange.

Although hexacyanometalate-based RFBs have shown promising electrochemical performances against the aforementioned issues, some unexpected degradation, such as leakage of electrolytes and precipitation as salts, may occur in the system, thereby facilitating the replacement or rebalancing the ratio of the active material solutions while maintaining the infra-tank and pump systems. To evaluate conceptual and technological potential, we prepared an intentionally degraded negolyte and replaced it with a new $K_3[Cr(CN)_6]$ solution as shown in Supplementary Fig. 5. Following the replacement, the specific capacity reaches the original performance after a couple of cycles for aging processes that are required to match the counterpart capacity with the posolyte. It is also recommended to adjust the posolyte and negolyte volume with maintaining a similar concentration at both sides in order to avoid water migration by osmotic pressure to design the commercially applicable RFBs. However, the solubilities of posolytes and negolytes do not generally correspond with each other, minimizing the overall energy density. Herein, we employed 0.4 M $K_3[Cr(CN)_6]$ as a negolyte because of the limited solubility of $K_4[Fe(CN)_6]$ used for the posolyte. Considering the solubility of $K_3[Cr(CN)_6]$ *per se*, up to 1.1 M

can be dissolved in water with 2 M NaCN supporting electrolytes. The solubility in water with 2 M NaCN supporting electrolyte was measured by fitting the UV-vis spectra as shown in Supplementary Fig. 6. The peak intensity of the fully saturated solution is 1.28014 at a wavelength of 432 nm. Compared to values at other concentrations of 0.05 to 0.4 M, we can deduce the unknown concentration to be approximately 1.1 M, allowing energy density beyond 30 Wh L^{-1} in our RFB system. Otherwise, according to previous studies, the solubility of ferrocyanide could increase to 1.5 M by cation exchange to ammonium ions, resulting in the high-energy density [36].

The outstanding properties of hexacyanometallates are not only limited to RFBs, possible exploring their application in a variety of ambitious projects. The main advantage of the $[Cr(CN)_6]^{4-/3-}$ redox system is the very low redox potential of the negolyte due to the coordination with strong-field ligands retaining high stability even against HER. A comparison against other well-known aqueous RFB systems (Fig. 5) shows that this high overall potential is contributed by the potential of the negolyte, $[Cr(CN)_6]^{4-/3-}$, suggesting a higher overall potential matching with high redox posolytes. We note that the low redox potential of $[Cr(CN)_6]^{4-/3-}$ will benefit from knowledge obtained by other electrochemical technologies, such as CO_2 electroreduction processes and biomass conversion [37]. Therefore, we believe that this invention will contribute significantly to stationary energy storage in other areas that prefer to combine with continuous-flow electroreduction systems.

Conclusion

In the quest for sustainable RFBs, we have discovered the new negolyte, $K_3[Cr(CN)_6]$, which exhibits a low redox potential of -1.15 V vs. SHE, stable cycling performance, and fast charge transfer kinetics. The coordination with strong-field ligands observed herein is expected to play important roles in governing the low-spin state of Cr^{II}, thereby allowing low redox potential during electrochemical cycling. On the basis of a wide variety of RFB chemistries beyond hexacyanometallates, our results, coupled with high stability and fast kinetics, will help to guide the development of RFBs with high-energy densities and prolonged lifetimes. Our thermodynamic DFT calculation also confirms that the cyanide-coordinated molecules can promote the fast kinetics attributed by virtue of their facile redox reaction *via* weak Jahn-Teller effects rather than the strong Jahn-Teller effects characterizing other compounds. The prototype full-cell configuration highlights a high-energy density of 11.4 Wh L^{-1} and a stable lifetime to 250 cycles when using a 0.4 M concentration of both active electrolytes. As $K_3[Cr(CN)_6]$ itself, it can dissolve up to approximately 1.1 M concentration, expecting to achieve a higher energy density than 20 Wh L^{-1} beyond the challenges in vanadium redox flow battery. Consequently, we believe that our new proposed $[Cr(CN)_6]^{4-/3-}$ systems represents a novel and scientifically intriguing material that can push forward the development of grid energy storage.

Methods

Synthesis of Potassium Hexacyanochromate ($K_3[Cr(CN)_6]$)

$K_3[Cr(CN)_6]$ was synthesized following a modified method based on previous literature [38,39]. $Cr(CH_3COO)_3$ (JUNSEI, Cr 21-25 %) was dissolved in 20 mL distilled (DI) water and this solution was transferred into a KCN (Alfa Aesar, 96.0 %) solution (8.93g of KCN in 30mL DI water). 0.24g of activated charcoal was added during the reaction After several minutes, activated charcoal was filtered and the filtered solution was partially dried in order to evaporate the remnant solvent. Finally, the solution was chilled to precipitate $K_3[Cr(CN)_6]$. This precipitated $K_3[Cr(CN)_6]$ was filtered and washed by ethanol five times, then dried in a vacuum oven at 40 ^oC. The synthesized $K_3[Cr(CN)_6]$ was characterized by XRD and compare with commercial $K_3[Cr(CN)_6]$ (Sigma Aldrich, 99.99%).

Half-cell characterization

Cyclic voltammetry (CV) measurements were conducted using an EC-Lab potentiostat (BioLogic). A three-electrode system was employed with an Ag/AgCl reference electrode filled with a 3 M KCl solution, Pt wire as a counter electrode, and a 3 mm diameter-glassy carbon working electrode. A half-cell test was performed using the 5 mM and 0.1 M solutions containing synthesized $K_3[Cr(CN)_6]$ with 1 M supporting electrolytes. To compare the redox reaction of chromium, we conducted experiments using the $CrCl_3$ redox system as a reference. 5 mM $CrCl_3$ (Sigma Aldrich, ≥ 98.0 %) was dissolved in DI water with the supporting electrolyte of 1 M HCl.

Flow cell (Full-cell) characterization

30 mL of $K_3[Cr(CN)_6]$ solution (0.1, 0.4, and 1 M) was used as an anolyte with 2 M NaCN (Alfa Aesar, 95 %) as the supporting electrolyte. As a catholyte, 0.15 M $K_3[Fe(CN)_6]$ (Sigma Aldrich, 99 %) and 0.3 M $K_4[Cr(CN)_6] \cdot 3H_2O$ (Sigma Aldrich, 98.5 % - 102.0 %) were dissolved in 2 M NaCl (Alfa Aesar, 99.0 %) supporting electrolyte, for which the total volume was 40 mL. The flow battery cell (TS CHEM) was assembled with 5 cm^2 (2 cm × 2.5 cm) carbon-felt electrode (XF-30a, TOYOBO), graphite plate, copper current collector, and Nafion membrane. Nafion (NRE-212, Sigma Aldrich, Nafion^{TM} perfluorinated membrane, thickness 0.002 inch) was soaked in a 0.1 M HCl solution for 30 min then rinsed in DI water. The carbon felt electrode was heated to 500 ^oC for 5 hrs under an air atmosphere. The anolytes and catholytes were circulated in a tube (Masterflex Norprene tubing, I.D 3.18 mm, O.D 6.35 mm) by pump drives (JenieWell, JWSE600) at an average flow rate of approximately 40 mL/min, where all carbon felt electrodes was compressed by ~70% in a stack cell.

A galvanostatic charge-discharge test was performed using an EC-Lab potentiostat at room temperature. Before taking measurements, we circulated both the anolyte and catholyte for 2 hrs without applying a bias. A constant current was applied during the charging and discharging processes (100 mA cm^{-2}) for a voltage cutoff range from 1 to 1.9 V. Power tests were conducted by potentiostat (IviumStat) at each

state of charge (SOC). Current scanning was employed during the discharging state in order to obtain peak power densities, which the cell was charged at a constant current density of 30 mA cm^{-2}.

The state of the anolyte during full-cell operation was investigated using UV-vis spectroscopy. The cell was charged at 30 mA cm^{-2} and discharged at 50 mA cm^{-2} from 1.0 to 1.9 V. We extracted 0.2 mL of the solution at each SOC (0 %, 25 %, 50 %, 75 %, and 100 %,) and diluted them 1/100 times (0.004 M).

Computational details

All first-principles calculations were conducted according to spin-unrestricted density functional theory (DFT) using the Gaussian 09 package [40]. Geometry optimizations and molecular orbital energy level calculations were carried out following Becke–Lee–Yang–Parr (B3LYP) hybrid functional [41] and the 6-31G basis set. The solvation effect of water was modeled using the integral equation formalism polarizable continuum model (IEFPCM). Various spin states from singlet to septet were considered and the state with the lowest DFT energy was selected for each molecule.

Solubility test

Various concentrations of $K_3[Cr(CN)_6]$ solution were prepared (0.05 M, 0.1 M, 0.2 M, 0.3 M, 0.4 M, and unknown (saturated solution)). The unknown solution was made by adding $K_3[Cr(CN)_6]$ into the 2M NaCN solution until the solid could no longer be dissolved, after which the residue was filtered. The concentration of the unknown solution was evaluated uinsg UV-visible spectroscopy. Absorbance is proportional to concentration. A pre-calibrated absorbance-concentration plot was obtained through the peak intensity at 429~432 nm for other solutions, and the solubility was calculated using this plot.

Declarations

Acknowledgments

This work was supported by the 2020 Research Fund (1.200115.01) of UNIST and Individual Basic Science & Engineering Research Program (NRF-2019R1C1C1009324) through the National Research Foundation of Korea funded by the Ministry of Science and ICT.

Author Contributions

J.J. and H.-W.L. conceived the idea, designed the experiments, and analyzed the data. J.J. and R.K. conducted all experiments with the assistance of C.L., S.K., J.R., S.J., J.C., and W.C. D.-H.S. completed DFT simulations. J.J., R.K., D.-H.S., and H.-W.L. interpreted the results. J.J., D.-H.S., and H.-W.L. co-wrote the paper. All authors discussed the results and commented on the manuscript.

Competing Interests

The authors declare no competing interest.

Data Availability

The data that support the plots within this paper and other findings of this study are available from the corresponding authors upon reasonable request.

Additional Information

Correspondence and requests for materials should be addressed to D.H.S. and H.W.L.

References

1. Yang, Z. *et al.* Electrochemical energy storage for green grid. *Chem. Rev.* **111**, 3577–3613 (2011).

2. Soloveichik, G. L. Flow Batteries: Current Status and Trends. *Chem. Rev.* **115**, 11533–11558 (2015).

3. Park, M., Ryu, J., Wang, W. & Cho, J. Material design and engineering of next-generation flow-battery technologies. *Nat. Rev. Mater.* **2**, (2016).

4. Yao, Y., Lei, J., Shi, Y., Ai, F. & Lu, Y. C. Assessment methods and performance metrics for redox flow batteries. *Nature Energy* (2021)

5. Yang, B., Jiang, H., Xie, J., Zhao, T. & Lu, Y. C. Diphenyl ditelluride as a low-potential and fast-kinetics anolyte for nonaqueous redox flow battery applications. *Energy Storage Mater.* **35**, 761–771 (2021).

6. Wang, W. *et al.* Recent progress in redox flow battery research and development. *Adv. Funct. Mater.* **23**, 970–986 (2013).

7. Parasuraman, A., Lim, T. M., Menictas, C. & Skyllas-Kazacos, M. Review of material research and development for vanadium redox flow battery applications. *Electrochim. Acta* **101**, 27–40 (2013).

8. LIVE Vanadium Price. https://www.vanadiumprice.com/ (2020).

9. Zeng, Y. K., Zhao, T. S., An, L., Zhou, X. L. & Wei, L. A comparative study of all-vanadium and iron-chromium redox flow batteries for large-scale energy storage. *J. Power Sources* **300**, 438–443 (2015).

10. Vesborg, P. C. K. & Jaramillo, T. F. Addressing the terawatt challenge: Scalability in the supply of chemical elements for renewable energy. *RSC Adv.* **2**, 7933–7947 (2012).

11. Lin, K. *et al.* Alkaline quinone flow battery. *Science.* **349**, 1529–1532 (2015).

12. Gong, K. *et al.* All-Soluble All-Iron Aqueous Redox-Flow Battery. *ACS Energy Lett.* **1**, 89–93 (2016).

13. Robb, B. H., Farrell, J. M. & Marshak, M. P. Chelated Chromium Electrolyte Enabling High-Voltage Aqueous Flow Batteries. *Joule* **3**, 2503–2512 (2019).

14. Ruan, W. *et al.* Designing Cr complexes for a neutral Fe-Cr redox flow battery. *Chem. Commun.* **56**, 3171–3174 (2020).

15. Schlesener, C. J., Amatore, C. & Kochi, J. K. Kinetics and Mechanism of Aromatic Oxidative Substitutions via Electron Transfer. Application of Marcus Theory to Organic Processes in the Endergonic Region. *J. Am. Chem. Soc* **106**, 3567–3577 (1984).

16. Johnson, D. A., Reid, M. A. & Electrochem, J. Chemical and Electrochemical Behavior of the Cr(III)/Cr(II) Half-Cell in the Iron-Chromium Redox Energy Storage System. *J. Electrochem. Soc.* **132**, 1058–1062 (1985).

17. Adin, A., Sykes, A. G., Gates, H. S. & Kin, E. L. The Chromium(II)-catalysed Dissociation of Monochlorochromium(III). *J. Chem. Soc. A* **80**, 1518–1521 (1966).

18. Zeng, Y. K., Zhao, T. S., Zhou, X. L., Zeng, L. & Wei, L. The effects of design parameters on the charge-discharge performance of iron-chromium redox flow batteries. *Appl. Energy* **182**, 204–209 (2016).

19. Bhatt, V. *Essentials of Coordination Chemistry*. *Academic Press* vol. 0 (2016).

20. Bae, C.-H., Roberts, E. P. L. & Dryfe, R. A. W. Chromium redox couples for application to redox flow batteries. *Electrochim. Acta* **48**, 279–287 (2002).

21. Bae, C., Roberts, E. P. L., Chakrabarti, M. H. & Saleem, M. All-chromium redox flow battery for renewable energy storage. *Int. J. Green Energy* **8**, 248–264 (2011).

22. Waters, S. E., Robb, B. H., Marshak, M. P. & Marshak, M. P. Effect of Chelation on Iron-Chromium Redox Flow Batteries. *ACS Energy Lett.* **5**, 1758–1762 (2020).

23. Yang, Y. *et al.* Quantitative measurement of cyanide released from Prussian Blue. *Clin. Toxicol.* **45**, 776–781 (2007).

24. Suo, L. *et al.* 'Water-in-salt' electrolyte enables high-voltage aqueous lithium-ion chemistries. *Science (80-.).* **350**, 938–943 (2015).

25. Hume, D. N. & Kolthoff, I. M. The Oxidation Potential of the Chromocyanide—Chromicyanide Couple and the Polarography of the Chromium Cyanide Complexes. *J. Am. Chem. Soc.* **65**, 1897–1901 (1943).

26. Nicholson, R. S. Theory and Application of Cyclic Voltammetry for Measurement of Electrode Reaction Kinetics. *Anal. Chem.* **37**, 1351–1355 (1965).

27. Chiang, A. & Adamson, A. W. Photochemistry of Aqueous $Cr(CN)_6^{3-}$. *J. Phys. Chem.* **72**, 3827–3831 (1968).

28. Wakefield, D. K., Schaap, W. B. & Wakefield2, D. K. Cyanoaquochromium(III) Complexes. Separation and Identification of the Neutral and Cationic Cyanoaquo Complexes of Chromium(III) and Aquation Kinetics of the Monocyanopentaaquochromium(III) Ion1. *Inorg. Chem.* **8**, 512–519 (1968).

29. Jeftić, L. & Feldberg, S. W. Chromium (II)-Catalyzed aquation of hexacyanochrornate (III) to pentacyanomonohydroxychromate(III). *J. Phys. Chem.* **75**, 2381–2387 (1971).

30. C. D. Wu, D. A. Scherson,* E. J. Calvo, and E. B. Y. A Bismuth-Based Electrocatalyst for the Chromous-Chromic Couple in Acid Electrolytes. *J. Electrochem. Soc.* **133**, 2109–2112 (1986).

31. Tseng, T.-M. *et al.* Carbon Felt Coated with Titanium Dioxide/Carbon Black Composite as Negative Electrode for Vanadium Redox Flow Battery. *J. Electrochem. Soc.* **161**, A1132–A1138 (2014).

32. Zhou, X. L., Zeng, Y. K., Zhu, X. B., Wei, L. & Zhao, T. S. A high-performance dual-scale porous electrode for vanadium redox flow batteries. *J. Power Sources* **325**, 329–336 (2016).

33. Jiang, H. R. *et al.* A high power density and long cycle life vanadium redox flow battery. *Energy Storage Mater.* **24**, 529–540 (2020).

34. Fornasiero, F. *et al.* Ion exclusion by sub-2-nm carbon nanotube pores. *PNAS* **105**, 17250–17255 (2008).

35. Lord, R. L. & Baik, M. H. Why does cyanide pretend to be a weak field ligand in $[Cr(CN)_5]^{3-}$? *Inorg. Chem.* **47**, 4413–4420 (2008).

36. Luo, J. *et al.* Unprecedented Capacity and Stability of Ammonium Ferrocyanide Catholyte in pH Neutral Aqueous Redox Flow Batteries. *Joule* **3**, 149–163 (2019).

37. Nitopi, S. *et al.* Progress and Perspectives of Electrochemical CO2 Reduction on Copper in Aqueous Electrolyte. *Chem. Rev.* **119**, 7610–7672 (2019).

38. Heintz, E. A. The synthesis of potassium hexacyanochromate (O). *J. Inorg. Nucl. Chem.* **21**, 262–264 (1961).

39. John H. B., J. C. B. *Inorganic Syntheses*. *McGraw-Hill Book Company, Inc.* vol. 2 (1946).

40. MJ Frisch, GW Trucks, HB Schlegel, M.J. Frisch, G.W. Trucks, H.B. Schlegel, G.E. Scuseria, M.A. Robb, J.R. Cheeseman, G. Scalmani, V. Barone, B. Mennucci, G. A. P. *Gaussian 09, Revision A. 02*. *Gaussian. Inc., Wallingford CT* (2016).

41. Lee, C., Yang, E. & Parr, R. G. Development of the Colic-Salvetti correlation-energy formula into a functional of the electron density. *Phys. Rev. B* **37**, 785–789 (1988).

Figures

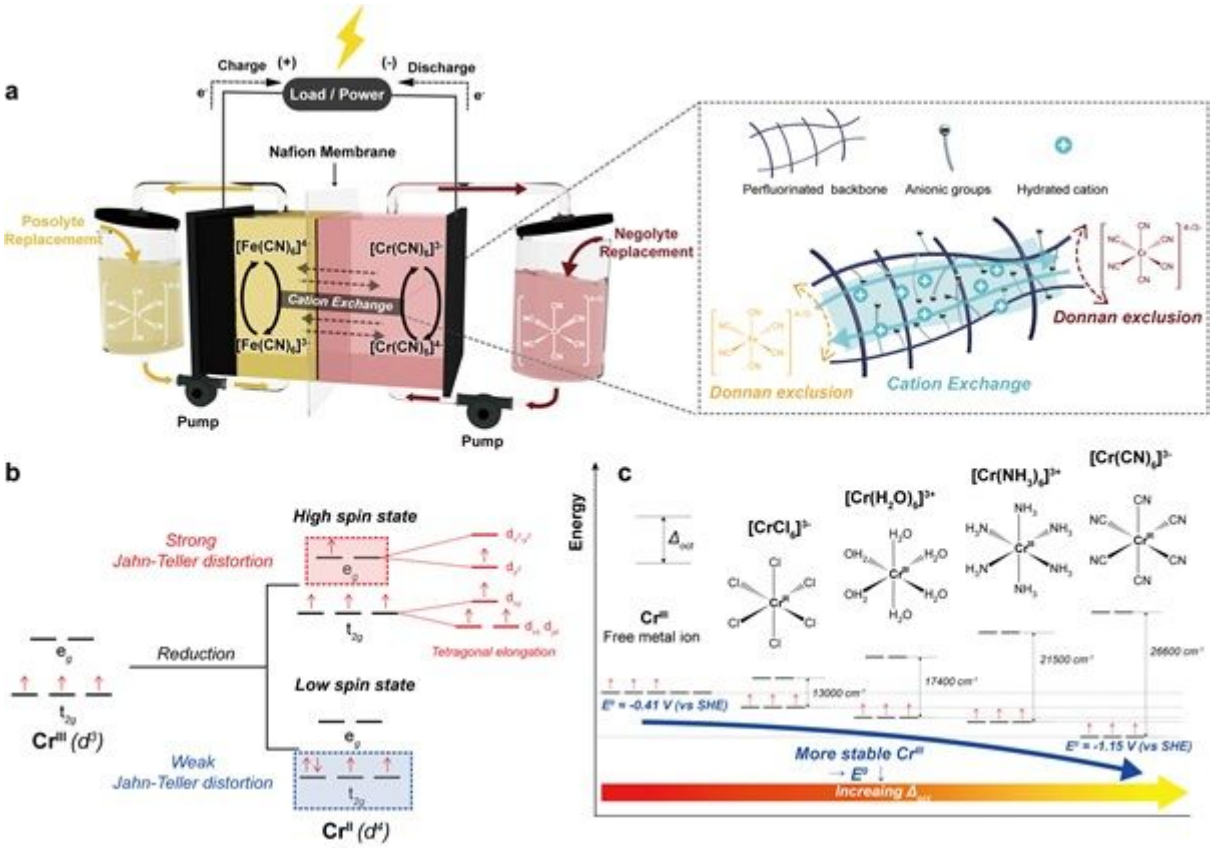

Figure 1

Cell configuration and d-orbital splitting for different chromium octahedral complexes. a, Cell schemetic of the negolyte of [Cr(CN)6]4-/3- paired with the posolyte of [Fe(CN)6]4-/3-. The negolyte (red) and posolyte (yellow) are circulated through the pump. The active electrolytes can be replaced or rebalanced when the system is degraded. Arrows in the middle of the diagram indicate cation migration across the Nafion membrane. Mobile cations of sodium are readily transported through the membrane. On the other hand, hexacyanometallate anions of [Cr(CN)6]4-/3- and [Fe(CN)6]4-/3- are excluded by Donnan exclusion effects. b, Jahn-Teller effects of CrII (d4) octahedral complex. c, d-orbital splittings and the reduction potentials of chromium-based octahedral complexes.

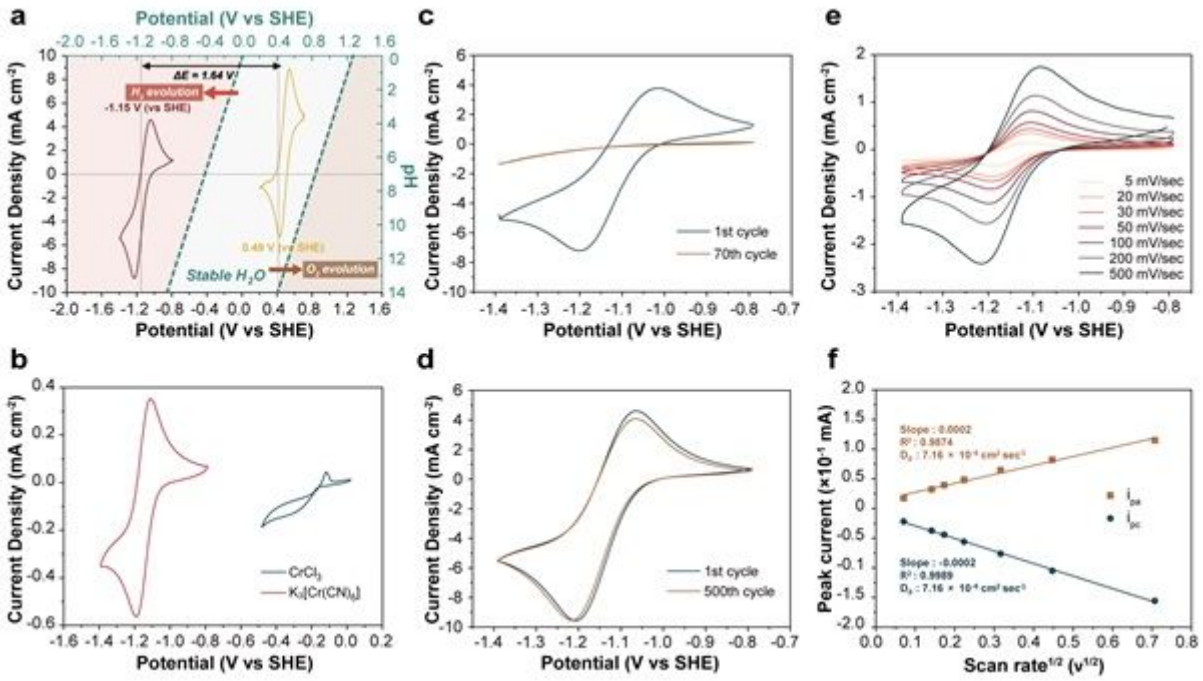

Figure 2

Electrochemical characterization of K3[Cr(CN)6]. a, Cyclic voltammogram (CV) of [Cr(CN)6]4-/3- redox species (brown) and the counterpart of [Fe(CN)6]4-/3- (yellow) at a scan rate of 20 mV s-1 on a glassy carbon electrode. Blue dashed lines denote the thermodynamic reduction potentials of HER and OER, which depend on pH. b, CV of [Cr(CN)6]4-/3- redox species (red) and the redox behavior of CrCl3 coordinated with weak-field ligands of chlorine (black) at a scan rate of 20 mV s-1. (c) to (d) Stability test of 0.1 M K3[Cr(CN)6] with the supporting electrolytes of (c) 1 M NaCl or (d) 1 M NaCN. e, CV curves of [Cr(CN)6]4-/3- redox species at different scan rates from 5 to 500 mV s-1. f, Relationship between peak currents and corresponding scan rates of K3[Cr(CN)6].

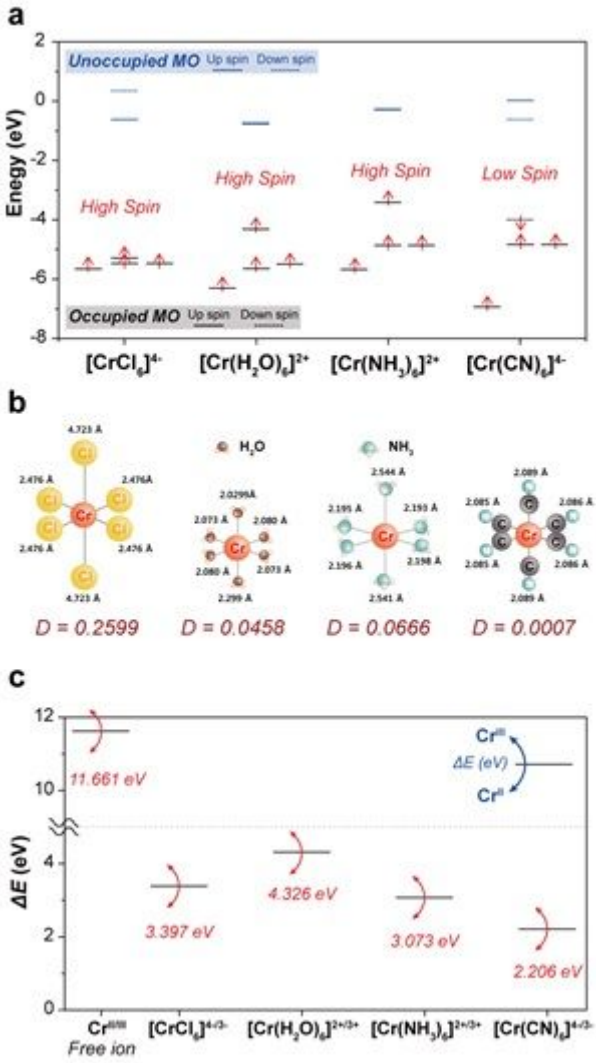

Figure 3

Simulated electronic configurations, Jahn-Teller distortions, and redox reaction energies of CrII-based compounds. a, Energy levels of electronic orbitals. Upward arrows represent electrons with up-spin and downward arrows represent electrons with down-spin. Black solid and dashed lines denote occupied molecular orbitals (MOs) for up-spin and down-spin, respectively. Blue solid and dashed lines indicate unoccupied MOs for up-spin and down-spin, respectively. b, Molecular structures with bond lengths of ligands and distortion index D of octahedral complex. c, Calculated energy changes during CrII/III redox reactions in these compounds.

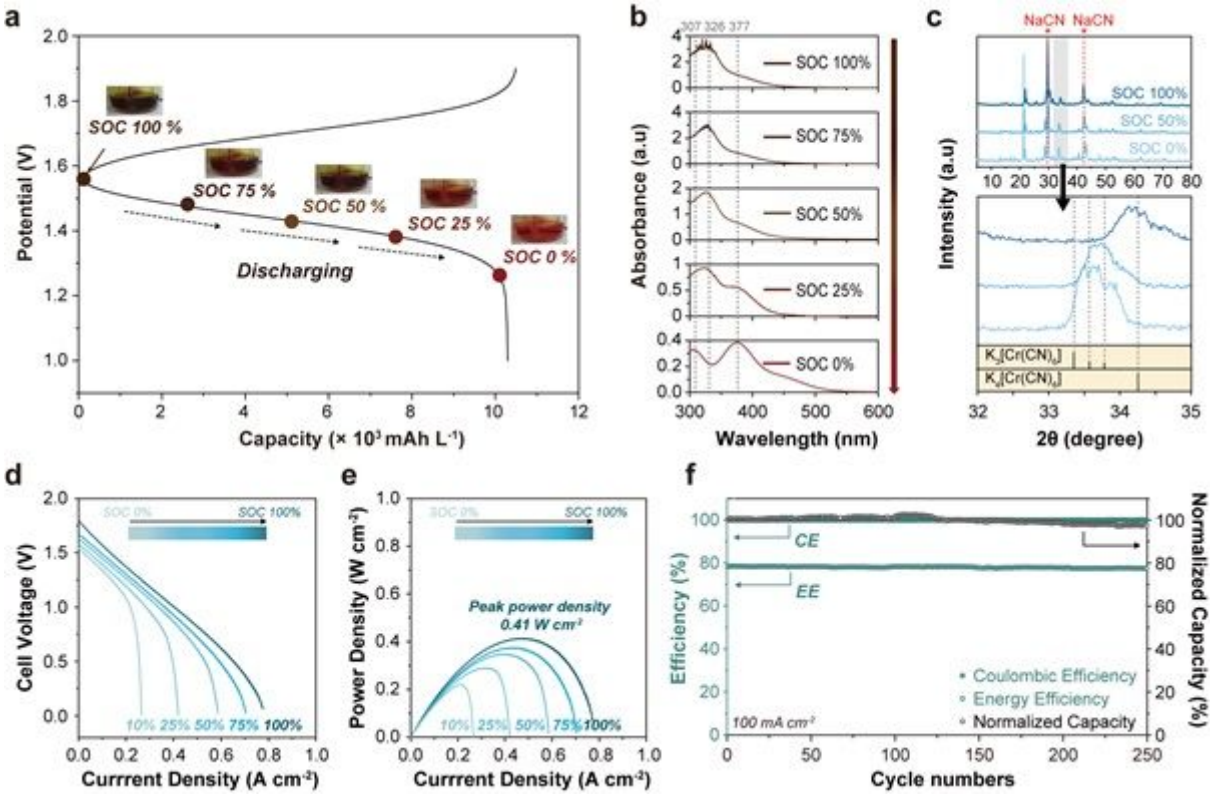

Figure 4

Full-cell performance. a, A typical voltage profile of K3[Cr(CN)6] and the corrdsponding solution images at different states of SOC (0 %, 25 %, 50 %, 75 %, and 100 %,). b, UV-vis spectra of K3[Cr(CN)6] at different states of of SOC (0 %, 25 %, 50 %, 75 %, and 100 %,). The single peak at 326 nm indicates the charged state of [Cr(CN)6]4- and the peaks at 307 and 377 nm denote the discharged state of [Cr(CN)6]3-. c, X-ray diffraction data of the post-mortem dried samples at SOC of 0 %, 50 %, and 100 %. d, Polarization curves and e, power density as a function of current density at the different states of SOC (0 %, 25 %, 50 %, 75 %, and 100 %). f, Plots of Coulombic efficiency, energy efficiency, and normalized capacity for 250 cycles. (±100mA cm-2)

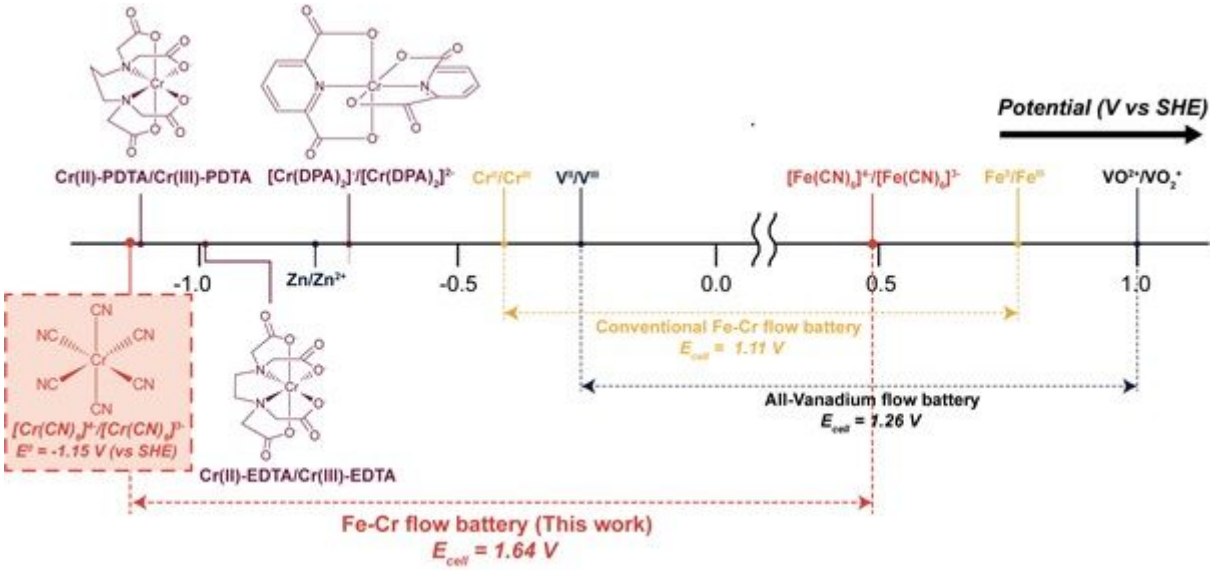

Figure 5

Standard redox potentials of aqueous redox flow batteries. All-vanadium systems possess relatively high potential region; this work covers the low redox potential of -1.15 V vs. SHE, which opens new avenues for the design of high-energy density RFBs.

Supplementary Files

This is a list of supplementary files associated with this preprint. Click to download.

- SupplementaryMaterialsNatureEnergy.docx
- Supplementaryvideo1Dischargingre.mp4